Franklin Open

A Novel Virtual Vector Modulation-based scheme of Model Power Predictive for VIENNA Rectifier

--Manuscript Draft--

Manuscript Number:	FRAOPE-D-23-00347
Article Type:	Original Research—Energy & Power Systems
Keywords:	Vienna rectifier; virtual vector modulation; model predictive direct power control; inductance parameters mismatch; fixed frequency
Corresponding Author:	Chaoliang Dang Department of Electrical Engineering., Xi'an University of Technology, Xi'an, CHINA
First Author:	Chaoliang Dang
Order of Authors:	Chaoliang Dang
	Yihua Wang
	Zehao Jiang
	Ding Liu
	Xiangqian Tong
	Wheeler Pat
Abstract:	When the finite control set model predictive(FCS-MPC) algorithm is applied to the three-level converter, there are problems such as large current harmonics, high requirements for the computing efficiency of the micro-controller, complex multi-objective optimization and limited output vector switching. In additional, the mismatch of inductance parameter may directly affect the observation accuracy of FCS-MPC. Furthermore, due to the limitation of finite set model prediction, it leads to the switching operation is not constant and the decrease of the grid-connected current quality. In this regard, an improved model predictive direct power control based on the combined virtual vector modulation (MPDPC-VM) is proposed by considering the influence of the filter inductance parameter mismatch. The finite control set and restricted vector switching of the Vienna rectifier are modeled to avoid excessive voltage jumps, and the predicted values of input power is obtained by the sliding-mode control (SMC) strategy. Then, a linear synthesis method of virtual vector modulation-based scheme is proposed, which increases the number of the available voltage vectors in a single switching period from 8 to 19. The grid-connected current ripple is improved by reducing the error between the expected voltage vector and the available voltage vector. Finally, the model reference adaptive system (MRAS) method is applied to improve the working reliability and reduce the influence of mismatching of inductance parameters. Extensive simulation and matching experimental results is given to demonstrate the validity of the proposed strategy under steady-state and transient responses conditions compared against the existing FCS-MPC.

Powered by Editorial Manager® and ProduXion Manager® from Aries Systems Corporation

Dear Editors:

As the first and corresponding author, Dr.Dang designed the experiment, conducted the data , carried out the theoretical simulation, and wrote the manuscript. Professor Liu is the postdoctoral supervisor of Dr.Dang. Professor Tong and Professor Wheeler. Pat provide theoretical support and experimental platform for the development of this study. YiHua WANG and ZeHao Jiang is responsible for reviewing the English grammar of the manuscript.No conflict of interest exist in the submission of this manuscript, and manuscript is approved by all authors for published previously, and not under consideration for publication elsewhere, in whole or in part. All the authors listed have approved the manuscript that is enclosed.

If you have any queries, please do not hesitate to contact me at the address below.

Corresponding author:
Chaoliang Dang
E-mail:dangclkk@163.com

Thank you and best regard.

Yours sincerely,

Chaoliang Dang

Ethical Statement

Title:A Novel Virtual Vector Modulation-based scheme of Model Power Predictive for VIENNA Rectifier

All Authors:Chao-Liang DANG, YiHua WANG, ZeHao Jiang, Ding LIU, Xiang-Qian TONG, Wheeler. Pat

I testify on behalf of all co-authors that our article submitted to Franklin Open

1) this material has not been published in whole or in part elsewhere;

2) the manuscript is not currently being considered for publication in another journal;

3)all authors have been personally and actively involved in substantive work leading to the manuscript, and will hold themselves jointly and individually responsible for its content.

No conflict of interest exist in the submission of this manuscript, and manuscript is approved by all authors for published previously, and not under consideration for publication elsewhere, in whole or in part.

I hope this paper is suitable for Franklin Open. We deeply appreciate your consideration of our manuscript, and we look forward to receiving comments from the reviewers as soon as possible. If you have any queries, please do not hesitate to contact me at the address below.

Corresponding author:
Chaoliang Dang
E-mail:dangclkk@163.com

Thank you and best regard.

Yours sincerely,

Chaoliang Dang

Manuscript Click here to view linked References

A Novel Virtual Vector Modulation-based scheme of Model Power Predictive for VIENNA Rectifier

Chao-Liang DANG[1,2,3], YiHua WANG[3], ZeHao Jiang[3], Ding LIU[1], Xiang-Qian TONG[3], Wheeler. Pat[4]

[a]*School of Automation and Information Engineering, Xi'an University of Technology, Xi'an 710048*
[b]*State Key Laboratory of Electrical Insulation and Power Equipment, Xi'an Jiaotong University, Xi'an 710049*
[c]*School of Electrical Engineering, Xi'an University of Technology, Xi'an 710054*
[d]*School of Electrical and Electronic Engineering, University of Nottingham, Nottingham, UK*

Abstract

When the finite control set model predictive(FCS-MPC) algorithm is applied to the three-level converter, there are problems such as large current harmonics, high requirements for the computing efficiency of the micro-controller, complex multi-objective optimization and limited output vector switching. In additional, the mismatch of inductance parameter may directly affect the observation accuracy of FCS-MPC. Furthermore, due to the limitation of finite set model prediction, it leads to the switching operation is not constant and the decrease of the grid-connected current quality. In this regard, an improved model predictive direct power control based on the combined virtual vector modulation (MPDPC-VM) is proposed by considering the influence of the filter inductance parameter mismatch. The finite control set and restricted vector switching of the Vienna rectifier are modeled to avoid excessive voltage jumps, and the predicted values of input power is obtained by the sliding-mode control (SMC) strategy. Then, a linear synthesis method of virtual vector modulation-based scheme is proposed, which increases the number of the available voltage vectors in a single switching period from 8 to 19. The grid-connected current ripple is improved by reducing the error between the expected voltage vector and the available voltage vector. Finally, the model reference adaptive system (MRAS) method is applied to improve the working reliability and reduce the influence of mismatching of inductance parameters. Extensive simulation and matching experimental results is given to demonstrate the validity of the proposed strategy under steady-state and transient responses conditions compared against the existing FCS-MPC.

***Index Terms*—Vienna rectifier; virtual vector modulation; model predictive direct power control; inductance parameters mismatch; fixed frequency**

1. INTRODUCTION

In recent years, the photoelectric and wind power have been vigorously promoted and developed because of their green and pollution-free advantages. How to reduce harmonic pollution of the power grid, improve the power quality and factor of electronic devices has become the key to the development of new energy technologies. Vienna rectifier can be used in DC charging system because of its advantages of high power density, no dead time and low power switching loss [1-3], and it is a three-phase power factor corrector with broad application prospects [5-7].With the development of microprocessors and control science, lot of nonlinear control algorithms have been widely used. Among these strategies, finite control set model predictive control (FCS-MPC) has gained widespread adoption in power electronics and motor control [3-5]. The fundamental concept behind FCS-MPC is to establish a value function with multiple objectives and systematically evaluate each voltage vector to identify the optimal one. As a versatile multi-objective approach, the effectiveness of FCS-MPC in fast dynamic response, multi-target tracking and nonlinear constraints has been verified[3-4,6]. Hence, it proves particularly suitable for controlling the strongly nonlinear VIENNA rectifier system (Fig.1)[6-12].

The operational mechanism of FCS-MPC control involves utilizing the discrete characteristics of the power electronic converter. A cost function is defined to assess all switching states of converters in each control cycle, and the optimal switching state becomes the control output vector. When applying traditional FCS-MPC strategy to three-level converter topology, it typically requires optimizing 27 switching states. This leads to a complex iterative optimization process. And also puts forward higher requirements for processor performance. To improve the above shortcomings, various control schemes have been proposed. These can be categorized into two main approaches. One approach utilizes FPGA's parallel computing capability and physical architecture for PWM modulation.Although it reduces the computational complexity of the processor , it does not fundamentally solve the cumbersome optimization process of FCS-MPC[10-14]. The other method simplifies the voltage vector set or reduces tracking targets by constructing a single objective function for controlling the three-level converter. However, it is difficult to achieve multi-target tracking, such as switching operation and balance control of positive and

negative voltage.It is difficult to optimize the value of weight factor because of the lack of direct mathematical relationship between weight factor and control variable.Overcoming the drawbacks of intricate optimization calculations and difficulties in selecting weighting factors caused by traditional FCS-MPC's inherent architecture while exploring multi-objective satisfactory optimization theory and implementation mechanisms are crucial aspects that need attention.

In [14], the objective value function is added to reduce the switching times, which effectively reduces the switching loss of the system. In [15], an improved method is proposed to obtain duty cycle by minimizing the root mean square of cost function, which achieved fixed switching frequency, but the effect was poor in multi-objective optimization. In [16], an improved algorithm with vector switching sequence was proposed for voltage source inverters, which can realize the fixed switching frequency, and reduced the output voltage ripple. Since the cost function of MPC is convenient to achieve multi-objective control, an additional weighting factors should be introduced to control the midpoint potential when the traditional FCS-MPC is adopted. However, the design of weighting factors is complicated, and there is no perfect design theory. In [17], by injecting zero sequence voltage to suppress the third order pulsating current signal, the neutral potential fluctuation is eliminated indirectly.In [18],the NP potential balance is realized by dynamically adjusting the action time of the redundant small vector and selecting the complex vector group Compared with the method of balancing the NP potential only by modulation factors, the fluctuation amplitude of NP potential by about 48%. An improved prediction algorithm based on redundant small vector is proposed to eliminate the fluctuation of DC-link voltage in [19].

The accuracy of model parameters is another key factor affecting the efficiency and performance of grid-connected converter. Consequently, the mismatch of model parameters will directly affect the grid-current performance, even cause system instability [7]. In [20], the relationship between reactive power components and inductance is used to construct an inductance observer in the power inner loop, and the change of inductance is observed in real time and system parameters are updated. In [21], a sensorless improved sliding mode observer (SMO) method is proposed for permanent magnet synchronous motor (PMSM) to observe the rotor position in real time. In [22], an online identification scheme of permanent magnet synchronous motor based on extended Kalman filter (EKF) is proposed, which can effectively observe the changes of stator resistance and flux linkage of the motor through formula calculation of the observed quantity. According to the above analysis, the research on the model parameter identification is mostly concentrated in the field of motor control system, and lack of the study on the grid-connected converters. At the same time, there is still a lack of analysis on the influence mechanism of model parameters. Meanwhile, due to the nonlinear characteristics of FCS-MPC, the evaluation method of parameter disturbance in the linear system is no longer applicable for the VIENNA rectifier.

In addition to the aforementioned analysis, current research on FCS-MPC primarily focuses on optimizing individual performance aspects such as variable switching frequency, balancing midpoint potential control, and simplified iterative optimization processes. However, this narrow focus significantly hinders the progress of predictive control in electric drive applications. There is still a need for an enhanced strategy that addresses the drawbacks of FCS-MPC, including complex optimization processes, difficulty in selecting of weighting factor and unfixed switching frequency.. Additionally, the influence of model parameters mismatch still exists. This paper selects the typical structure of a three-level AC/DC Vienna rectifier as the subject of study. To address these issues, An improved model predictive control scheme MPDPC-VM is proposed by combining FCS-MPC with virtual vector modulation strategy.Firstly, the general analytical expressions of model parameter mismatch and grid-current performance are established, and a direct power prediction algorithm by considering parameter mismatch is proposed. Secondly, the number of optional voltage vectors in each sampling period is increased to reduce the error between the predicted and the reference value. The voltage vector is further accurately divided to effectively reduce the control set to reduce the computation burden of the processor, and the balance control of neutral potential is realized by selecting redundant small vectors. Then, the inductance parameters identification based on the model reference adaptive system (MRAS) is proposed to improve the robustness of system and the necessary verification analysis is carried out.

2. MATHEMATICAL MODEL OF VIENNA RECTIFIER

As illustrated in Fig. 1, the current of inductance L in phase x is represented by i_{gx} (where x can be a, b, or c), while u_{gx} denotes the electromotive force of the power grid. The filter inductor is denoted as L, and D_{xp} and D_{xn} define the diode rectifier bridge. S_{x1} and S_{x2} are bidirectional switching units, whereas C_1 and C_2 refer to the dc-link filter capacitors. It should be noted that both C_1 and C_2 have an equal capacitance value denoted as C. Lastly, u_{dc} defines the output voltage of the dc-link.

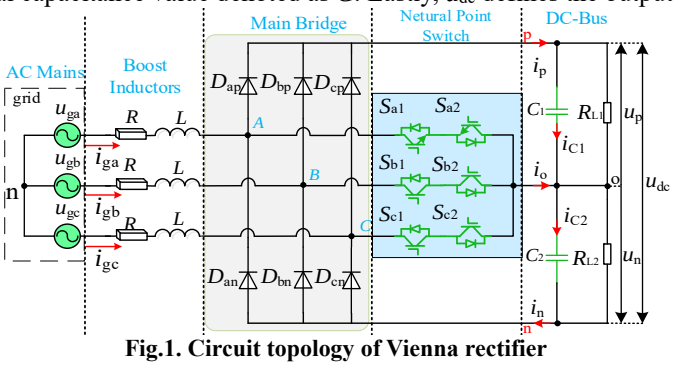

Fig.1. Circuit topology of Vienna rectifier

Fig.2 illustrates the voltage vector diagram in space for the VIENNA rectifier. This diagram can be categorized into four

groups based on magnitudes and spatial positions, namely zero vectors, small vectors, medium vectors, and large vectors.

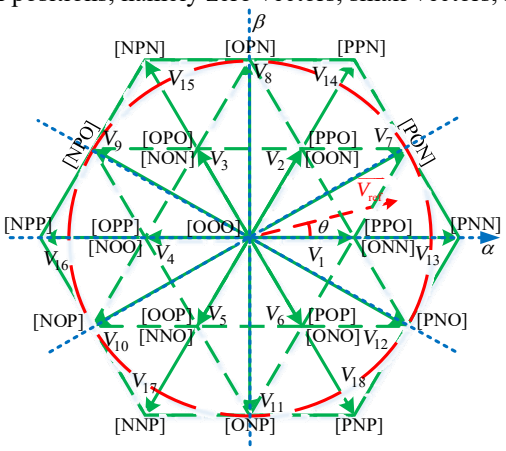

Fig.2 Space voltage vector distribution diagram of Vienna rectifier.

3. WORKING PRINCIPE OF THE MPDPC

3.1 The principle of model predictive direct power control

Based on the theory of instantaneous power, the calculation is performed to determine the active power and reactive power. By applying Kirchhoff's voltage law, we can express the equation for balancing phase voltages on the AC side as follows:

$$\begin{cases} L\dfrac{\mathrm{d}i_{\mathrm{ga}}}{\mathrm{d}t}=u_{\mathrm{ga}}-Ri_{\mathrm{ga}}-u_{\mathrm{aN}} \\ L\dfrac{\mathrm{d}i_{\mathrm{gb}}}{\mathrm{d}t}=u_{\mathrm{gb}}-Ri_{\mathrm{gb}}-u_{\mathrm{bN}} \\ L\dfrac{\mathrm{d}i_{\mathrm{gc}}}{\mathrm{d}t}=u_{\mathrm{gc}}-Ri_{\mathrm{gc}}-u_{\mathrm{cN}} \end{cases} \tag{1}$$

The expression of u_{xn} described in (3) is

$$\begin{bmatrix} u_{\mathrm{aN}} \\ u_{\mathrm{bN}} \\ u_{\mathrm{cN}} \end{bmatrix}=u_{\mathrm{p}}\begin{bmatrix} S_{\mathrm{ap}}-\dfrac{1}{3}\sum\limits_{k=a,b,c}S_{\mathrm{kp}} \\ S_{\mathrm{bp}}-\dfrac{1}{3}\sum\limits_{k=a,b,c}S_{\mathrm{kp}} \\ S_{\mathrm{cp}}-\dfrac{1}{3}\sum\limits_{k=a,b,c}S_{\mathrm{kp}} \end{bmatrix}+u_{\mathrm{n}}\begin{bmatrix} -S_{\mathrm{an}}+\dfrac{1}{3}\sum\limits_{k=a,b,c}S_{\mathrm{kn}} \\ -S_{\mathrm{bn}}+\dfrac{1}{3}\sum\limits_{k=a,b,c}S_{\mathrm{kn}} \\ -S_{\mathrm{cn}}+\dfrac{1}{3}\sum\limits_{k=a,b,c}S_{\mathrm{kn}} \end{bmatrix} \tag{2}$$

The mathematical model of the system can be simplified by transforming the three-phase stationary coordinate system into a two-phase stationary coordinate system through coordinate transformation. Subsequently, the expression with disorganization is presented as follows:

$$\begin{cases} L\dfrac{i_{\mathrm{g}\alpha}(k+1)-i_{\mathrm{g}\alpha}(k)}{T_s}=u_{\mathrm{ga}}(k)-Ri_{\mathrm{g}\alpha}(k)-u_{\alpha\mathrm{N}}(k) \\ L\dfrac{i_{\mathrm{g}\beta}(k+1)-i_{\mathrm{g}\beta}(k)}{T_s}=u_{\mathrm{g}\beta}(k)-Ri_{\mathrm{g}\beta}(k)-u_{\beta\mathrm{N}}(k) \end{cases} \tag{3}$$

According to the instantaneous power theory, the instantaneous active and reactive power of the AC side of the system in the two-phase $\alpha\beta$ stationary coordinate system is calculated:

$$\begin{bmatrix} p \\ q \end{bmatrix}=\begin{bmatrix} u_{\mathrm{ga}} & u_{\mathrm{g}\beta} \\ u_{\mathrm{g}\beta} & -u_{\mathrm{ga}} \end{bmatrix}\begin{bmatrix} i_{\mathrm{g}\alpha} \\ i_{\mathrm{g}\beta} \end{bmatrix} \tag{4}$$

Take the derivative of both sides of Equation (3), and calculate the rate of change of active and reactive power on the network side, as shown in (4):

$$\begin{cases} \dfrac{\mathrm{d}p}{\mathrm{d}t}=u_{\mathrm{g}\alpha}\dfrac{\mathrm{d}i_{\mathrm{g}\alpha}}{\mathrm{d}t}+i_{\mathrm{g}\alpha}\dfrac{\mathrm{d}u_{\mathrm{g}\alpha}}{\mathrm{d}t}+u_{\mathrm{g}\beta}\dfrac{\mathrm{d}i_{\mathrm{g}\beta}}{\mathrm{d}t}+i_{\mathrm{g}\beta}\dfrac{\mathrm{d}u_{\mathrm{g}\beta}}{\mathrm{d}t} \\ \dfrac{\mathrm{d}q}{\mathrm{d}t}=u_{\mathrm{g}\beta}\dfrac{\mathrm{d}i_{\mathrm{g}\alpha}}{\mathrm{d}t}+i_{\mathrm{g}\alpha}\dfrac{\mathrm{d}u_{\mathrm{g}\beta}}{\mathrm{d}t}-u_{\mathrm{g}\beta}\dfrac{\mathrm{d}i_{\mathrm{g}\beta}}{\mathrm{d}t}-i_{\mathrm{g}\beta}\dfrac{\mathrm{d}u_{\mathrm{g}\alpha}}{\mathrm{d}t} \end{cases} \tag{5}$$

Under the condition of ideal grid voltage, the Vienna rectifier grid side voltage relation is shown as (5), where ω is the

grid voltage angular frequency. By differentiating both sides of (5), the change rate of the grid-voltage of the Vienna rectifier at time *t* can be obtained, as shown in (6):

$$\begin{cases} \dfrac{\mathrm{d}u_{g\alpha}}{\mathrm{d}t} = -\omega u_{g\beta} \\ \dfrac{\mathrm{d}u_{g\beta}}{\mathrm{d}t} = \omega u_{g\alpha} \end{cases} \tag{6}$$

Eq. (3) and (6) are substituted into (4). Through calculation and sorting, the change rate of active power *p* and reactive power *q* at time *t* can be obtained:

$$\begin{cases} \dfrac{\mathrm{d}p}{\mathrm{d}t} = \dfrac{1}{L}(u_{g\alpha}^2 + u_{g\beta}^2 - u_{g\alpha}u_{\alpha o} - u_{g\beta}u_{\beta o}) - \omega q \\ \dfrac{\mathrm{d}q}{\mathrm{d}t} = \dfrac{1}{L}(u_{g\alpha}u_{\beta o} - u_{g\beta}u_{\alpha o}) + \omega p \end{cases} \tag{7}$$

Since the sampling period is much less than the period of the grid voltage, for an ideal grid, the following predicted values of the active and reactive power at the of the system can be obtained by the first-order forward Euler method, as shown in (7), where $p^{\mathrm{p}}(k+1)$ and $q^{\mathrm{p}}(k+1)$ represent the predicted values of the active and reactive power, respectively.

The resistance *R* in (1) is ignored. Combined with (6) and (7), the predicted values of the input active and reactive power $p^{\mathrm{p}}(k+1)$ and $q^{\mathrm{p}}(k+1)$ can be obtained as:

$$\begin{cases} p^{p}(k+1) = p(k) - \omega T_s q(k) + \dfrac{T_s}{L}(u_{g\alpha}^2 + u_{g\beta}^2 - u_{g\alpha}u_{\alpha o} - u_{g\beta}u_{\beta o}) \\ q^{p}(k+1) = q(k) + \omega T_s p(k) + \dfrac{T_s}{L}(u_{g\alpha}u_{\beta o} - u_{g\beta}u_{\alpha o}) \end{cases} \tag{8}$$

When the traditional model predictive direct power control(MPDPC) is adopted, additional terms need to be added to the objective function to balance the voltage of the neutral point of the DC bus, as shown in (9).

$$g(i) = (p^{*} - p^{p}(k+1))^2 + (q^{*} - q^{p}(k+1))^2 + \lambda(u_{\mathrm{p}}(k+1) - u_{\mathrm{n}}(k+1))^2 \tag{9}$$

Where, $u_{\mathrm{p}}(k+1)$ and $u_{\mathrm{n}}(k+1)$ represent the predicted voltage values of upper and lower capacitors of the dc-link.

As shown in the eq.3, the different values of the weighting factor λ have a great influence on the neutral point potential and the grid-current. Due to there is no direct mathematical relation between λ and the control variables, the value of weighting factors difficulty to selected. In this paper, the objective function $g(i)$ is designed according to the power change minimization standard. Each vector in the candidate vector set is evaluated in the objective function to obtain the voltage vector corresponding to the minimum value, that is, the optimal vector. Where, p_{ref}^{*} and q_{ref}^{*} respectively represent the reference values of active power and reactive power, in this paper, the reference value of reactive power q^{*} is 0. The minimum sum of squares of the power error is used as the optimal index, and the cost function adopted is as follows:

$$g(i) = \left[p_{\mathrm{ref}}^{*}(k) - p(k+1) \right]^2 + \left[q_{\mathrm{ref}}^{*}(k) - q(k+1) \right]^2 \tag{10}$$

3.2. Design method of voltage loop base on the SMC

The output signal from the voltage control loop in the Vienna rectifier serves as the prescribed signal for direct power control, significantly influencing the stability and reliability of the system. Due to the parameter design of PI controller depends on the load resistance and circuit parameters.Rapid variations on the load side can result in suboptimal control performance regarding the DC side voltage. In light of these considerations, an enhanced voltage loop design, leveraging Sliding Mode Control (SMC), is implemented. In accordance with the circuit topology of the Vienna rectifier, the ensuing equation is derived:

$$\begin{cases} C_1 \dfrac{\mathrm{d}u_{\mathrm{p}}}{\mathrm{d}t} = i_{g\alpha}s_{\alpha p} + i_{g\beta}s_{\beta p} - \dfrac{u_{\mathrm{dc}}}{R_{\mathrm{L}}} \\ C_2 \dfrac{\mathrm{d}u_{\mathrm{n}}}{\mathrm{d}t} = -i_{g\alpha}s_{\alpha n} - i_{g\beta}s_{\beta n} - \dfrac{u_{\mathrm{dc}}}{R_{\mathrm{L}}} \end{cases} \tag{11}$$

Assuming the system is operating at unity power factor, the ensuing mathematical representation can be formulated as follows:

$$\begin{cases} p^{*} = p_{ac} = p_{dc} \\ p_{dc} = u_{\mathrm{dc}}i_{\mathrm{dc}} = \dfrac{1}{2}u_{\mathrm{dc}}C\dfrac{\mathrm{d}u_{\mathrm{dc}}}{\mathrm{d}t} + \dfrac{{u_{dc}}^2}{R_{\mathrm{L}}} \end{cases} \tag{12}$$

By simplifying (12), the following expression can be obtained:

$$\frac{\mathrm{d}u_{\mathrm{dc}}}{\mathrm{d}t} = -4\frac{u_{\mathrm{dc}}}{CR_L} + 4p/C \tag{13}$$

The sliding surface function is selected as:

$$\begin{cases} S_1 = K_1(q^* - q) \\ S_2 = K_2(u_{dc}^{*2} - u_{dc}^{2}) + \dfrac{d}{dt}(u_{dc}^{*2} - u_{dc}^{2}) \end{cases} \tag{14}$$

For the specified system, the dc side voltage reference signal remains constant, thereby inducing system dynamics along the trajectory defined by $\boldsymbol{S}$=0 on the sliding mode surface. By substituting (14) into (13), the ensuing derivation is as follows:

$$p^* = Ck(u_{dc}^{*2} - u_{dc}^{2}) / 4 + u_{dc}^{2} / R_L \tag{15}$$

4. MPDPC-VM SCHEME WITH INDUCTANCE PARAMETERS ONLINE IDENTIFICATION

4.1Virtual vector modulation-based scheme

Model predictive direct power control (MPDPC) can realize multi-objective control, which has the advantages of fast dynamic response, multi-target tracking and a small amount of calculation. Within each sampling period, a meticulous evaluation of the value function is conducted for every switch state within the designated sector. The optimal switch state, minimizing the cost function value, is then meticulously chosen and implemented during the subsequent control period. Because the choice of switching state is only related to the cost function, the switching frequency is not fixed, resulting in the grid current ripple and harmonic is very large [21-23].

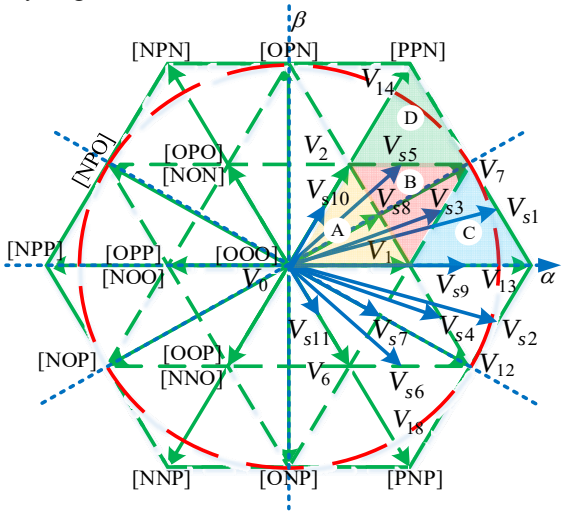

Fig. 3 MPDPC-VM presented

To address the identified limitations, this paper introduces a fixed-frequency MPDPC-VM method approach. In conventional MPDPC strategies, each sector is constrained to seven voltage vectors, resulting in a substantial deviation between the anticipated and actual voltage vectors. The realization method of DSVM strategy is to combine two basic voltage vectors into virtual vectors according to the parallelogram rule in a sampling period. The synthesis principle of virtual vectors in sector I is illustrated in Fig. 3, where a virtual vector is formed through a linear combination of two real vectors with identical activation times during a switching period.Consequently, 13 virtual vectors can be derived from the original 7 real vectors, evenly distributed across the vector plane. By adhering to the parallelogram rule, virtual vectors can be linearly synthesized through the simultaneous action of two basic vectors within a given period.For example, as depicted in Fig.3, consider the virtual vectors in sector I.Obviously, the virtual vectors V_{s5} is synthesized by V_2 and V_7, and the switching time are T_1 (0.5T_s) and T_2 (0.5T_s), respectively. In the MPDPC-VM strategy, virtual voltage vectors are synthesized from basic voltage vectors, and the number of voltage vectors can be selected in a sector is increased, which improves the quality of grid-current. The rearranged representation of the virtual vector in Figure 4 is as follows:

$$\begin{cases} V_m{}^v = \sum\limits_{i=1,2} d_i V_r \\ T_1 + T_2 = T_s \end{cases} \tag{16}$$

Where, V_r denote the original voltage vector (As shown in the Fig.4), T_1 and T_2 is vector switching time.

When located in sectors I, the virtual vector synthesis method presented is shown as Table. I.

Table. I

VIRTUAL VECTORS IN SECTOR I

Virtual vectors	Compound method	Duty ratio
V_{s1}	0.5V_{13}+0.5V_7	0.5,1,0.5
V_{s2}	0.5V_{13}+0.5V_{12}	0.5,0.5,1
V_{s3}	0.5V_1+0.5V_7	0.5,1,0

V_{s4}	$0.5V_1+0.5V_{12}$	0.5,0,1
V_{s5}	$0.5V_1+0.5V_2$	0,1,0.5
V_{s6}	$0.5V_{12}+0.5V_6$	0,0.5,1
V_{s7}	$0.5V_0+0.5V_{12}$	0,0.5,0.5
V_{s8}	$0.5V_0+0.5V_7$	0,0.5,0
V_{s9}	$0.5V_1+0.5V_{13}$	0,0,0.5
V_{s10}	$0.5V_0+0.5V_2$	0,0,0.5
V_{s11}	$0.5V_0+0.5V_6$	0,0,0.5

Take the sector-I as an example, A pair of positive and negative small vectors have the same effect on the line voltage, but it has the opposite polarity on the neutral point current. The introduction of a surplus small vector results in a midpoint current with reversed polarity, as depicted in Fig.4. Specifically, the positive small vector [POO] induces the charging of the upper capacitor, C_1, thereby elevating its potential. Conversely, the negative small vector [ONN] causes the lower capacitor C_2 to reduce the potential of C_2.The effect on the neutral point potential is in the opposite state.

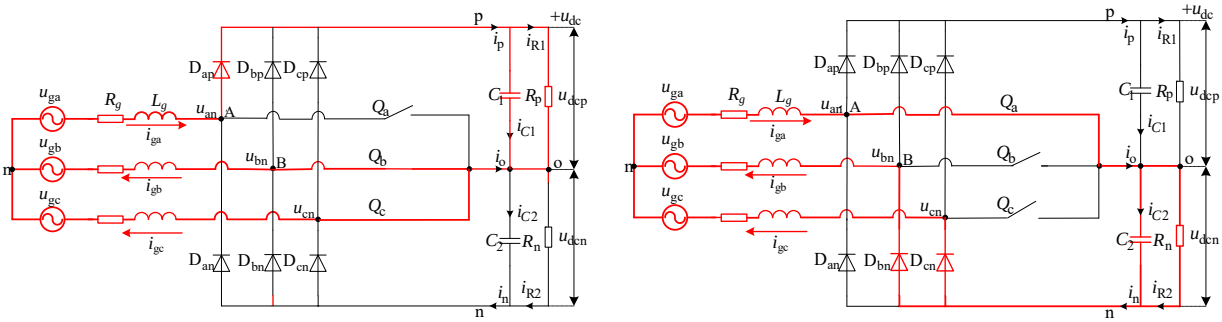

(a)[POO] **(b) [ONN]**

Fig.4 Action of positive and negative vectors

By comparing u_p and u_n, it is divided into two switching states according to the type of redundant small vectors. The selection principle of control set in the sector-I is shown in TABLE II.

TABLE II.

SELECTION PRINCIPLE OF VECTOR SET

Sector	Switching state	I_O	Dc bus capacitance status
1	POO	-Ic	
2	PPO	-Ic	C_1 (recharge)
3	OPO	Ib	
4	OPP	-Ia	
5	OOP	Ic	C_2 (discharge)
6	POO	-Ib	
1	ONN	-Ia	
2	OON	Ic	C_1 (discharge)
3	NON	-Ib	
4	NOO	Ia	
5	NNO	-Ic	C_2 (recharge)
6	ONO	Ib	

The virtual vectors V_{s3} and V_{s4} synthesized from small vectors when neutral point potential equilibrium is considered are different from the virtual vector synthesis method shown in Table II. Table III delineates the synthesis methodology employed for virtual vectors V_{s3} and V_{s4} within Sector I.

Table.III

VIRTUAL VECTORS V_{s3}, V_{s4} IN SECTOR I

Virtual vectors	Compound method	Switching Time
V_{s3}	$0.5V_2+0.5V_{13}$	$0.5T_s$, $0.5T_s$, 0
V_{s4}	$0.5V_6+0.5V_{13}$	$0.5T$s, 0, $0.5T_s$

4.2 On-line identification of inductance parameters

Due to the aging of equipment or the difference of manufacturing technology level, the nominal value of system parameter nameplate may not match the actual parameter [23-27], that is, the error between the nominal value of filter inductance parameter L_m and the actual parameter L_0 will directly influence the grid-current performance, and even cause instability. To improve the robustness to the parameter mismatch, this paper establishes the influence mechanism and mathematical model of filter inductance on grid-current performance with considering the parameter mismatch, as shown in the (17):

$$\triangle i = \frac{\triangle L T_s}{L_0(L_0+\triangle L)}[(u_{gx}(k)-u_g(k)-Ri(k)] = \frac{\triangle L T_s}{L_0 L_m}[(u_{gx}(k)-u_g(k)-Ri(k)] \tag{17}$$

Where, ΔL is the disturbance quantity of filter inductor; L_0 is the initial value of filter inductor; L_m is the actual value of inductance parameter; $u_{gx}(k)$ and $u_g(k)$ are the ideal value and sampling value of grid voltage, respectively.

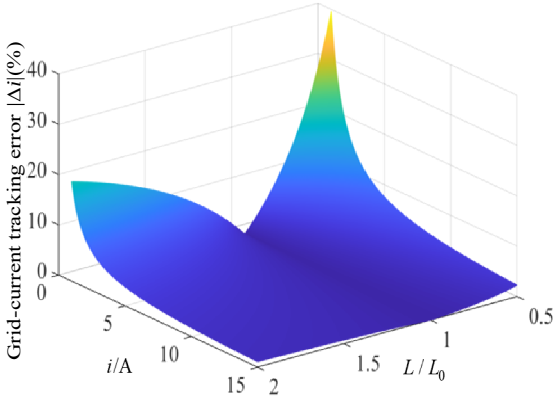

Fig.5 Influence of inductance parameters on prediction accuracy of grid- current.

Take the Vienna rectifier built in this paper as an example. The switching frequency is 50kHz, the model inductance parameter is 0.5mH, the parasitic resistance is 0.1 Ω , and the grid voltage error is assumed to be 10V and in phase with the current. The influence on the prediction accuracy with the changes of filter inductance parameters and grid current is shown as Fig.5. Clearly, the prediction error is not only related to the disturbance of resistance and the filter inductance, but also depends on the instantaneous value of the grid-current and voltage vector. When the model inductance parameters is larger than the actual value, the current tracking error may be increased rapidly with the decrease of the inductance ratio.

The error between the nominal value of the filter inductance parameter L_0 and the actual parameter L_m will cause the model mismatch and directly affect the grid current performance. In order to improve the robustness of parameter mismatch, the on-line inductance parameter identification method is proposed and the influence of the inductance parameter mismatch on the grid current performance is analyzed in this paper. Eq. (18) is the mathematical model under the dq coordinate axis

$$\begin{cases} L_m \dfrac{i_d(k+1)-i_d(k)}{T_s} = L_m \omega i_q(k) + u_{gd}(k) - u_{cd}(k) \\ L_m \dfrac{i_q(k+1)-i_q(k)}{T_s} = L_m \omega i_d(k) + u_{gq}(k) - u_{cq}(k) \end{cases} \tag{18}$$

Then, the current change of *dq* axis in a control cycle can be shown by (19).

$$\begin{cases} \Delta i_d = \dfrac{T_s}{\Delta L}\left[\omega i_q(k) + u_{gd}(k) - u_{cd}(k)\right] \\ \Delta i_q = \dfrac{T_s}{\Delta L}\left[\omega i_d(k) + u_{gq}(k) - u_{cq}(k)\right] \end{cases} \tag{19}$$

Where, Δi_d、Δi_q are the *dq* axis current variation components, u_{gd} (*k*) and u_{gq} (*k*) are the grid voltages, and u_{cd} (*k*) and u_{cq} (*k*) are the input voltages of the VIENNA rectifier. According to the theoretical analysis shown in (19), the change of current is directly related to the error value of inductance ΔL . When the actual inductance value L_m is inconsistent with the reference inductance value L_0, the inductance error value will be generated, which will lead to the fluctuation of grid current.

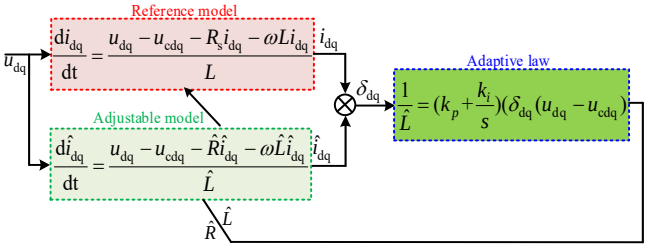

Fig.6 Theoretical block diagram with MARS

According to the principle of reference adaptive, the expression equations of reference model and adjustable model are derived, as shown in (20).

$$\begin{cases} \hat{\boldsymbol{i}} = \hat{\boldsymbol{H}}\hat{\boldsymbol{i}} + \hat{N}\hat{\boldsymbol{u}} + \hat{M}\hat{\boldsymbol{z}} \\ \hat{N} = \dfrac{1}{\hat{L}} \\ \hat{M} = -\dfrac{1}{\hat{L}} \\ \hat{\boldsymbol{H}} = \begin{bmatrix} 0 & \varpi \\ -\varpi & 0 \end{bmatrix} \\ \hat{\boldsymbol{i}} = \begin{bmatrix} i_d \\ i_q \end{bmatrix},\ \hat{\boldsymbol{u}} = \begin{bmatrix} u_{gd} \\ u_{gq} \end{bmatrix},\ \hat{\boldsymbol{z}} = \begin{bmatrix} u_{cd} \\ u_{cq} \end{bmatrix} \end{cases} \tag{20}$$

Combined with the reference model and the adjustable model expression, the error expression is:

$$\dot{\varepsilon} = \boldsymbol{H}\varepsilon + (\boldsymbol{H} - \hat{\boldsymbol{H}})\hat{\boldsymbol{i}} + (N - \hat{N})\boldsymbol{u} + (M - \hat{M})\boldsymbol{z} \tag{21}$$

By simplifying (21), the complete feedback system can be deduced as follows:

$$\begin{cases} \dfrac{\mathrm{d}\varepsilon}{\mathrm{d}t} = \boldsymbol{H}\varepsilon + W_1 = \boldsymbol{H}\varepsilon - W \\ W_1 = -W \\ W = -(\boldsymbol{H} - \hat{\boldsymbol{H}})\hat{\boldsymbol{i}} + (N - \hat{N})\boldsymbol{u} + (M - \hat{M})\boldsymbol{z} \end{cases} \tag{22}$$

In order to keep the nonlinear time-varying system stable, according to popov's super-stability theory, the system can keep stable only when the following conditions are met:

$$\eta(0,t) = \int_0^t z^T \omega \mathrm{d}t \geq -r^2 \tag{23}$$

Where, r is a finite positive number.

According to the model reference inductance adaptive structure, the adaptive rate ($1/\boldsymbol{L} - 1/\hat{\boldsymbol{L}}$) can be assumed as the proportional differential structure as shown in the (24):

$$\frac{1}{L} - \frac{1}{\hat{L}} = \int_0^t R_1(\tau)\mathrm{d}\tau + R_2(\tau) \tag{24}$$

Then the adaptive rate can be written as:

$$\eta(0,t) = \int_0^t (\int_0^t R_1(\tau)d\tau + R_2(\tau))[\varepsilon_{\mathrm{d}}(u_{\mathrm{sd}} - u_{\mathrm{cd}}) + \varepsilon_{\mathrm{q}}(u_{\mathrm{sq}} - u_{\mathrm{cq}})]\mathrm{d}t = \eta_1(0,t) + \eta_2(0,t) \geq -r^2 \tag{25}$$

In order to keep the system stable, the designed adaptive rate needs to meet the following conditions:

$$\begin{cases} \eta_1(0,t_1) = \int_0^t \int_0^t R_1(\tau)\mathrm{d}\tau[\varepsilon_{\mathrm{d}}(u_{\mathrm{sd}} - u_{\mathrm{cd}}) + \varepsilon_{\mathrm{q}}(u_{\mathrm{sq}} - u_{\mathrm{cq}})]\mathrm{d}t \geq -r_1^2 \\ \eta_2(0,t) = \int_0^t \int_0^t R_2(\tau)\mathrm{d}\tau[\varepsilon_{\mathrm{d}}(u_{\mathrm{sd}} - u_{\mathrm{cd}}) + \varepsilon_{q}(u_{\mathrm{sq}} - u_{\mathrm{cq}})]\mathrm{d}t \geq -r_2^2 \end{cases} \tag{26}$$

Under the condition of stability, the final adaptive rate of inductance can be expressed in (27).

$$\hat{L} = 1/(\frac{1}{L_0} + \int_0^t k_i[(i_{\mathrm{d}} - \hat{i}_{\mathrm{d}})(u_{\mathrm{gd}} - u_{\mathrm{cd}}) + (i_{\mathrm{q}} - \hat{i}_{\mathrm{q}})(u_{\mathrm{gq}} - u_{\mathrm{cq}})]d\tau + k_p(i_{\mathrm{d}} - \hat{i}_{\mathrm{d}})(u_{\mathrm{gd}} - u_{\mathrm{cd}}) + (i_{\mathrm{q}} - \hat{i}_{\mathrm{q}})(u_{\mathrm{gq}} - u_{\mathrm{cq}})] \tag{27}$$

5.RESULTS AND DISCUSSION

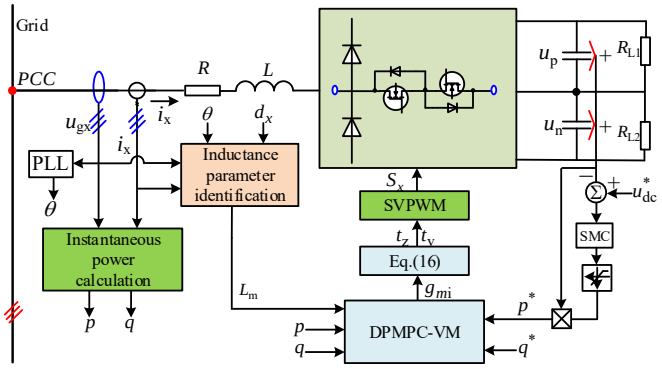

Fig.7 Block diagram with the presented MPDPC-VM control strategy

In this part, the basic structure of the presented MPDPC-VM strategy regulating system which involves a voltage loop SMC controller and inner loop MPDPC will be introduced as described in the Fig.7.The virtual vector is linearly synthesized from the real vector according to the parallelogram rule, the voltage vectors in each sector are increased from 8 to 19, the cost function values under 19 different voltage vectors are calculated, and the switching state with the minimum cost function is selected. The flowchart of the Vienna rectifier with the MPDPC-VM method adopted is shown in the Fig.8.

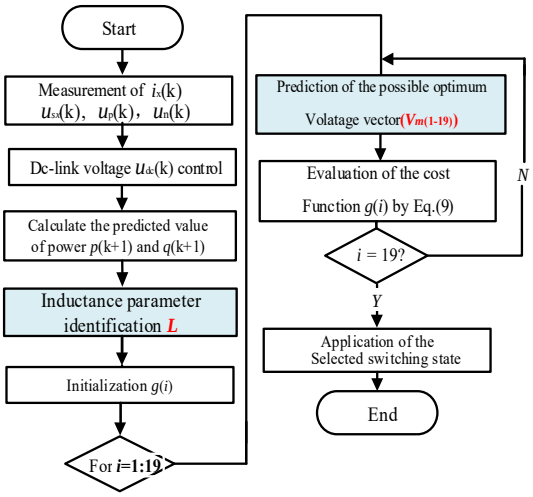

Fig.8 Flow diagram of the proposed MPDPC-VM

5.1 Simulation results discussion

This study conducts a comparative analysis and simulation of the MPDPC-VM against the conventional MPDPC method using the Matlab/Simulink simulation platform. The objective is to substantiate the superior performance of the proposed MPDPC-VM control strategy. The pertinent parameters are meticulously delineated in Table IV. It is imperative to emphasize that, unless explicitly stated otherwise, a uniform sampling frequency of 20 kHz and a simulation step size of 2e-6 are employed across all simulation scenarios. For the sake of clarity and brevity, only phase A is taken as an example to illustrate the simulation results.

Table.IV

CIRCUIT PARAMETERS INVOLVED

Parameter	Description	Values
U_{gx},V/Hz	Grid voltage	380/50
L_0,H	Given value of control	0.0025
L_g, H	Inductance	0.005
C_1 and C_2 ,uF	dc-link bus capacitor	1080
T_s ,s	Sampling time	0.00005
u_{dc} ,V	dc-link voltage	800
$R_{L1}$and R_{L2}, Ω	Loads	40

Fig.9(a) illustrates the grid current waveform as the filter inductance transitions from 0.00025H to 0.0005H at 0.3s. With an increase in filter inductance, there is a notable attenuation of the grid-connected current ripple.However, the grid current waveform has obvious distortion without inductance parameters identification after 0.3s. In contrast, Fig. 9(b) depicts the grid current response when introducing filter inductor parameter identification. Evidently, the incorporation of online identification for inductance parameters leads to a substantial enhancement in the quality of the grid current. This observation serves as a compelling validation of the accuracy and efficacy of the parameter identification theory expounded in this paper.

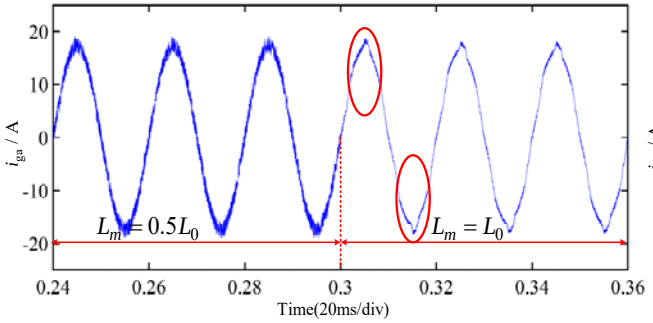

(a)*Without inductor identification*

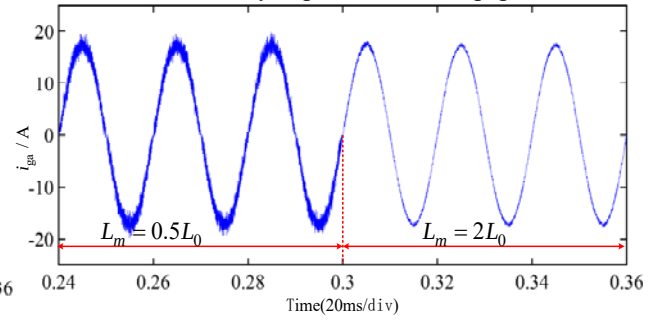

(b) *With identification*

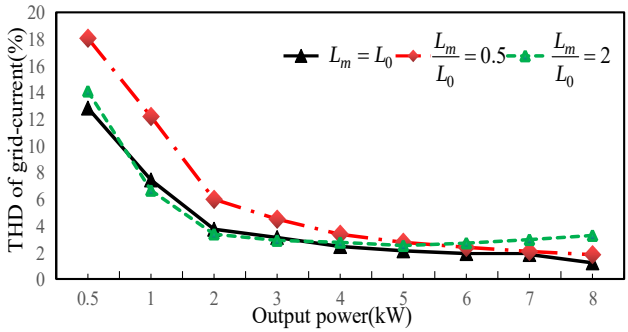

(c)THD of grid-current under different inductance parameter mismatch and power

Fig.9 Simulation results of inductance mismatch

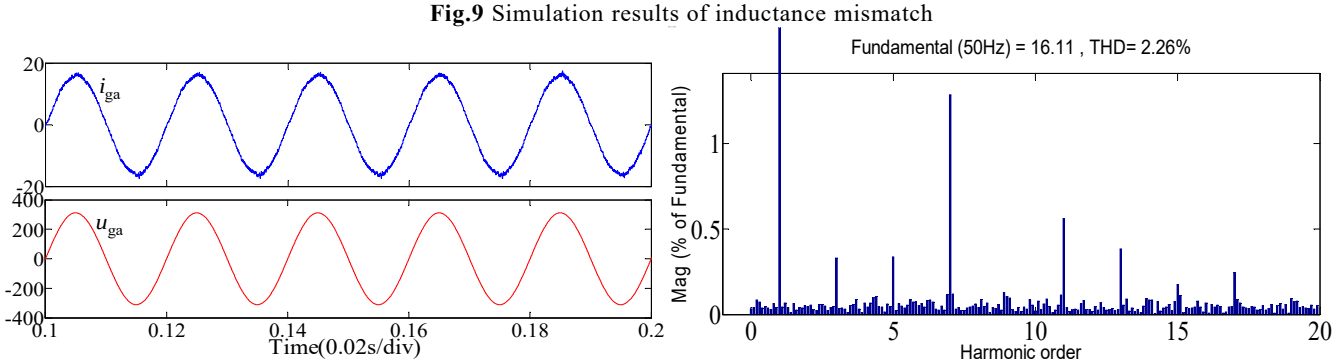

(a) *MPDPC*

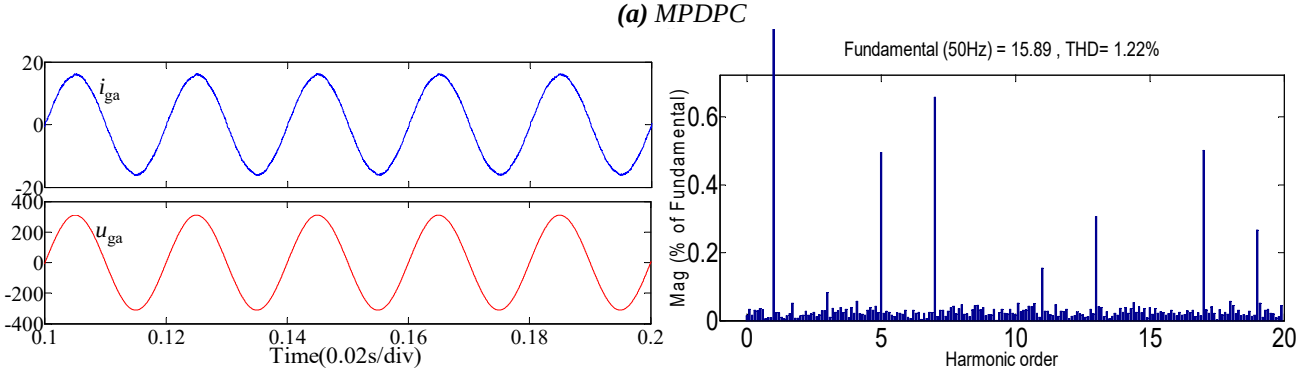

(b) *MPDPC-VM*

Fig.10 Steady-state simulation waveform with different control strategy.

The simulation results pertaining to grid-current under rated power operating conditions are depicted in Fig.10. Evidently, the grid current waveform in Fig. 10(a) exhibits a marginal deviation compared to its counterpart in Fig. 10(b). Upon closer examination, it is observed that the Total Harmonic Distortion (THD) of the grid current experiences a reduction of 1.04% when employing the proposed MPDPC-VM,, signifying its unequivocal superiority over the conventional MPDPC strategy in identical operational scenarios.

The simulation outcomes under half-power conditions with the implementation of the proposed MPDPC-VM and the conventional MPDPC control strategy are illustrated in Fig. 11(a) and Fig. 11(b), respectively. Upon examination, it is observed that the Total Harmonic Distortion (THD) of the power grid-current, as influenced by MPDPC-VM, exhibits a reduction of 1.69%.

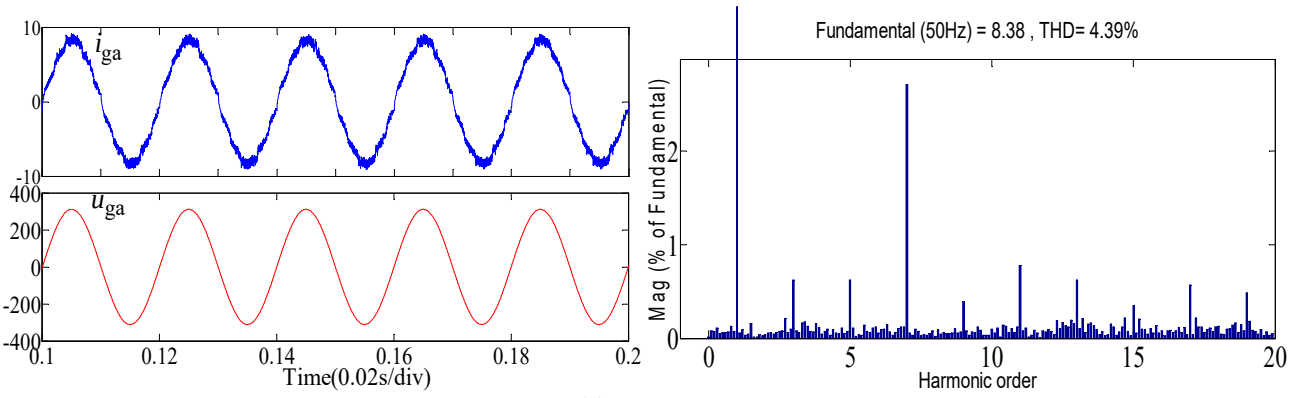

(a) *MPDPC*

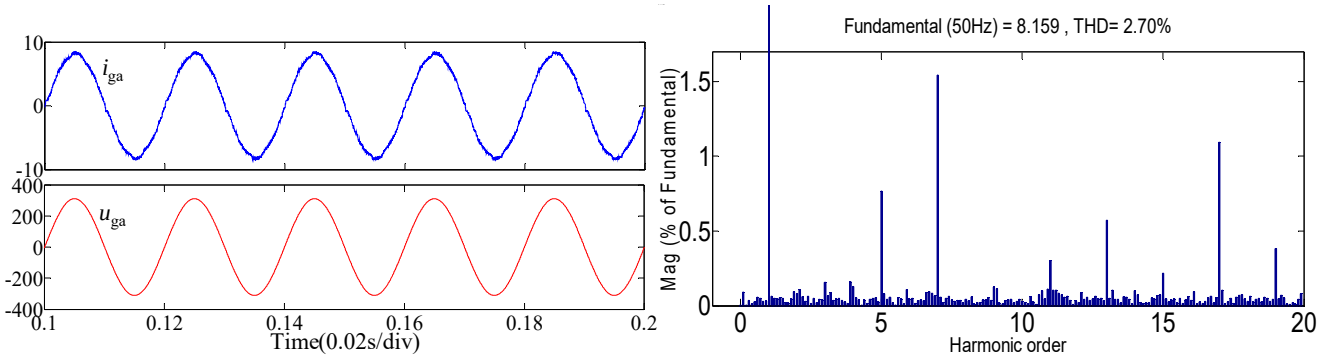

***(b)** MPDPC-VM*

Fig.11 Steady-state simulation waveform with different control method when operated in half power.

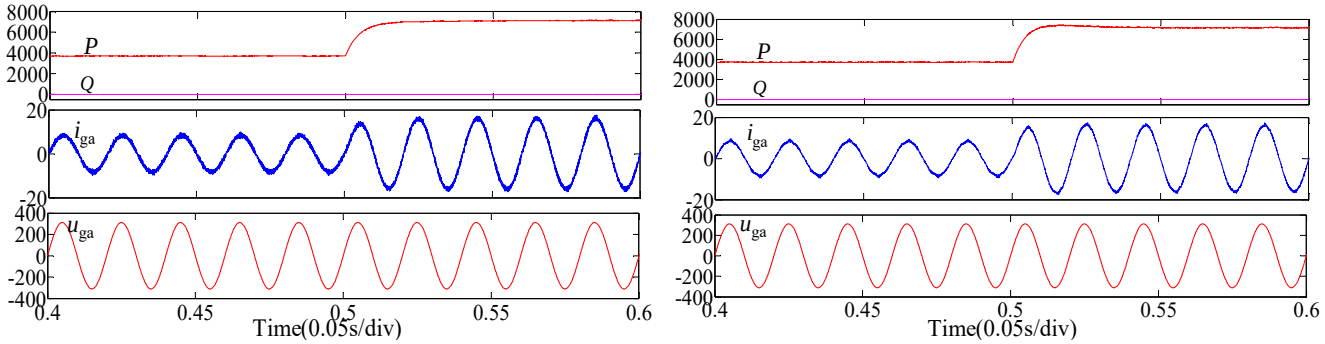

***(a)** MPDPC* ***(b)** MPDPC-VM*

Fig.12 Transient simulation waveform with different control strategy.

The transient response under various control strategies is illustrated in Fig.12. It can be seen from the simulation waveform that both active power and grid-current can quickly track the reference value, and the dynamic performance is good. Nevertheless, a detailed examination of Fig. 12(a) and Fig. 12(b) exposes that the grid-current response under conventional MPDPC exhibits notable ripple and distortion at the peak of current, resulting in inferior waveform quality compared to MPDPC-VM.

5.2 Discussion of experiment results

In light of theoretical analysis and consideration of circuit parameters, we have constructed a hardware-in-the-loop experimental platform utilizing the PLECS-BOX (refer to Fig. 13(a)) and a Vienna rectifier experimental setup (depicted in Fig. 13(b)). The simulation and experimental parameters have been meticulously aligned with the findings of theoretical analysis. The efficacy of the proposed MPDPC-VM strategy is rigorously examined in comparison to the conventional MPDPC control method. This scrutiny encompasses a comprehensive analysis of grid-current harmonics and dynamic response. The experimental results are shown in Fig.14-18.

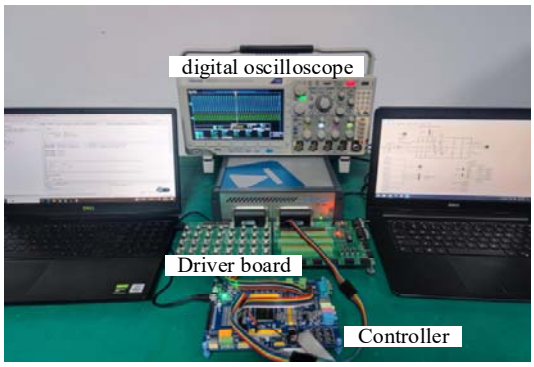

***(a)** PLECS-BOX*

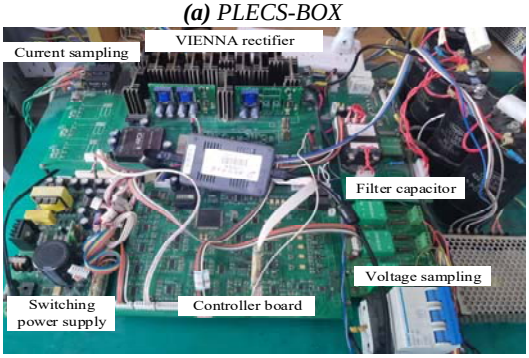

***(b)**Experimental platform*

Fig.13 Experimental platform.

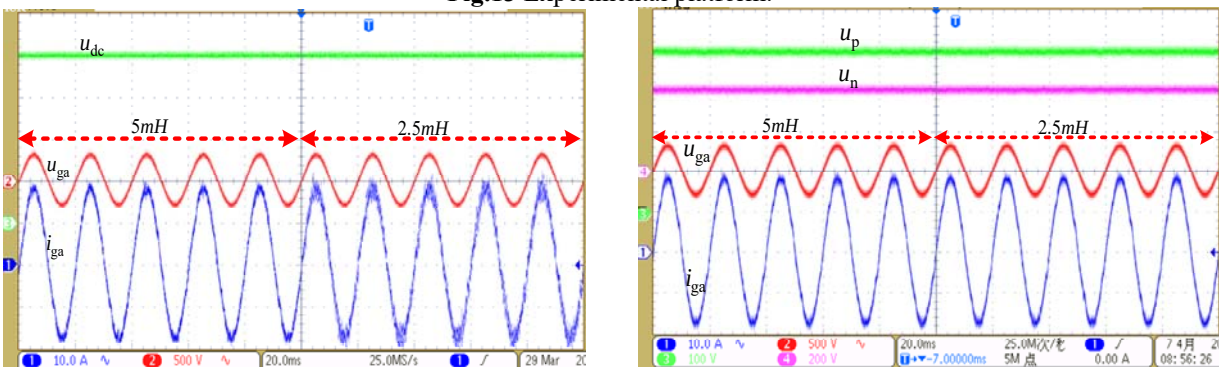

(a) Without inductor identification *(b)*. With identification

Fig.14 Results of inductance mismatch.

Fig.14 shows the input current waveform when the filter inductance changes from 0.005H to 0.0025H (When the experimental verification is carried out, the inductance value is changed through the form of parallel inductance. When the inductance parameter identification is not introduced, the default value of filter inductance is 0.005H, while the actual inductance value is 0.0025H. When the inductance parameter identification is adopted, the inductance value is 0.0025H, and is always consistent with the actual inductance value). It is evident that without introducing the filter inductance parameter, there is a noticeable distortion in the performance of the grid-current waveform. The utilization of filter inductor parameter identification proves to be instrumental in enhancing the quality of the grid current. The obtained results robustly validate the accuracy and efficacy of the parameter identification theory put forth in this study.

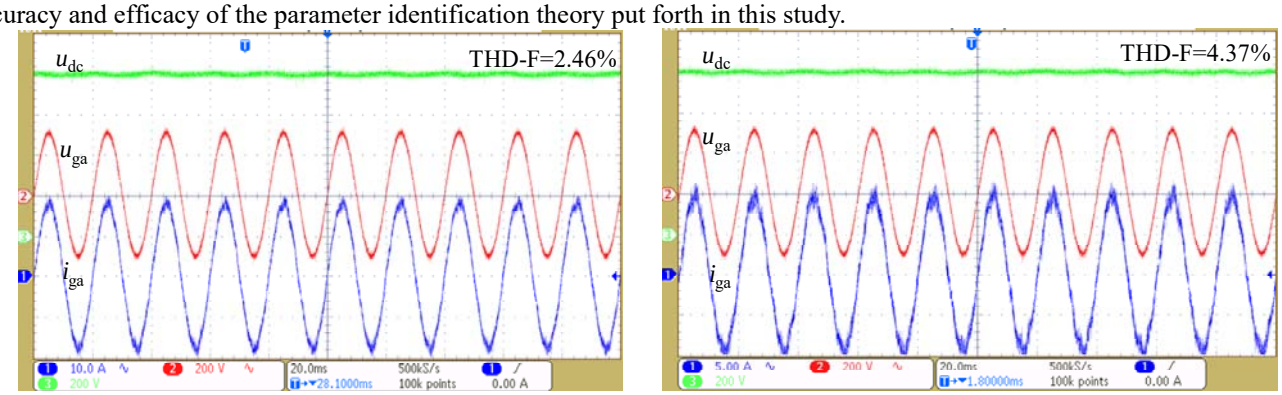

(a)Full power ***(b)Half power***

Fig.15 Static response waveform with MPDPC.

The grid current performance, as characterized by the MPDPC, exhibited values of 2.46% and 4.37%. Clearly, the peak value of grid-current with the traditional MPDPC is slightly distorted and the current ripple increases significantly. In contrast, the implementation of the MPDPC-VM yields a substantial improvement in grid current ripple. This outcome serves as a compelling validation of the efficacy of the novel MPDPC-VM introduced in this study.

In contrast to the conventional MPDPC, the graph depicted in Fig. 16 illustrates the grid current response under both half-load and full-load conditions when the MPDPC-VM adopted. The total harmonic distortion (THD) of the grid-current registers approximately 1.27% and 2.35%, respectively. The utilization of the MPDPC-VM strategy leads to a substantial enhancement in grid-current ripple, thereby unequivocally showcasing the efficacy of the proposed MPDPC-VM.

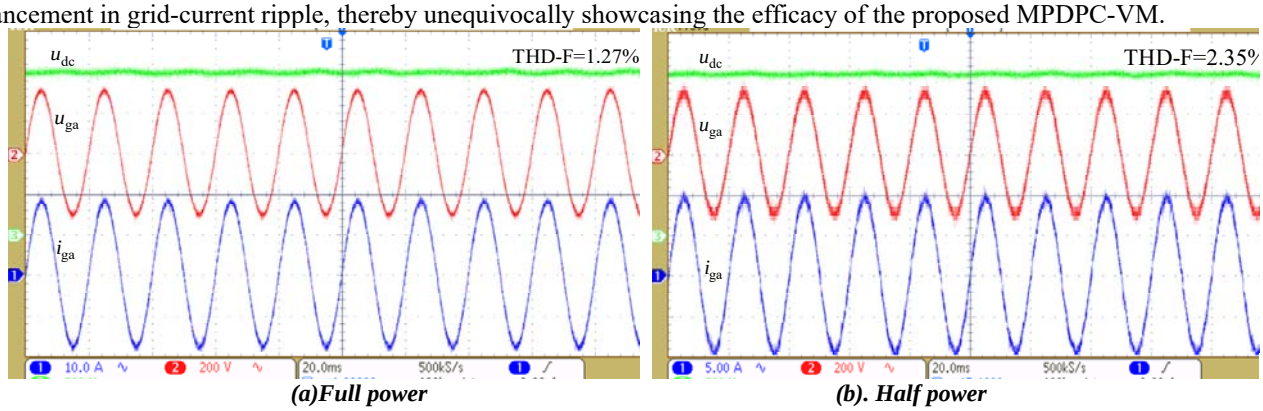

(a)Full power ***(b). Half power***

Fig.16 Static response waveform with MPDPC-VM.

Fig.17 shows the response when the system output power changed under MPDPC and MPDPC-VM control. It is evident that both grid current and active power exhibit rapid tracking of the reference values. The transient response time for the current to attain a new stable state is notably less than 0.05 seconds, even with a 50% change in load.Nevertheless, the conventional MPDPC method demonstrates larger current ripple and noticeable waveform distortion. In contrast, the MPDPC-VM strategy yields reduced current harmonic content and a smaller current ripple.

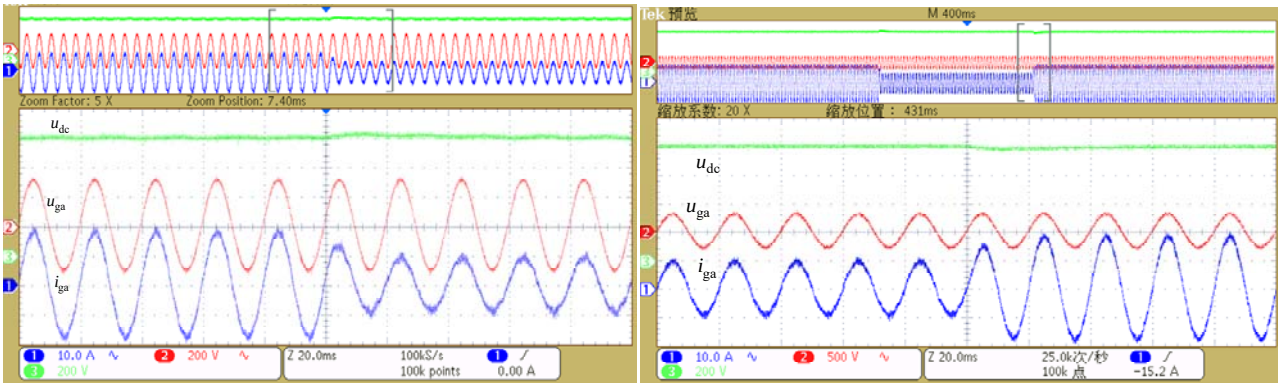

(a) MPDPC ***(b) MPDPC-VM***

Fig.17 Experiment result when the load changed.

The waveforms illustrated in Fig. 18 depict the positive and negative dc-link output voltage waveforms, as well as the grid voltage and current output waveforms of phase A. Where u_o=u_p-u_n, the neutral point potential fluctuation with the traditional FCS-MPC is 15.4V, while the fluctuation is predicted to be around 3.6V based on the MPDPC-VM.This reduction highlights the enhanced performance achieved through the adoption of MPDPC-VM in the present study.The experimental validation demonstrates the efficacy of the proposed method in maintaining neutral point balance. he experimental results are consistent with the simulation results.

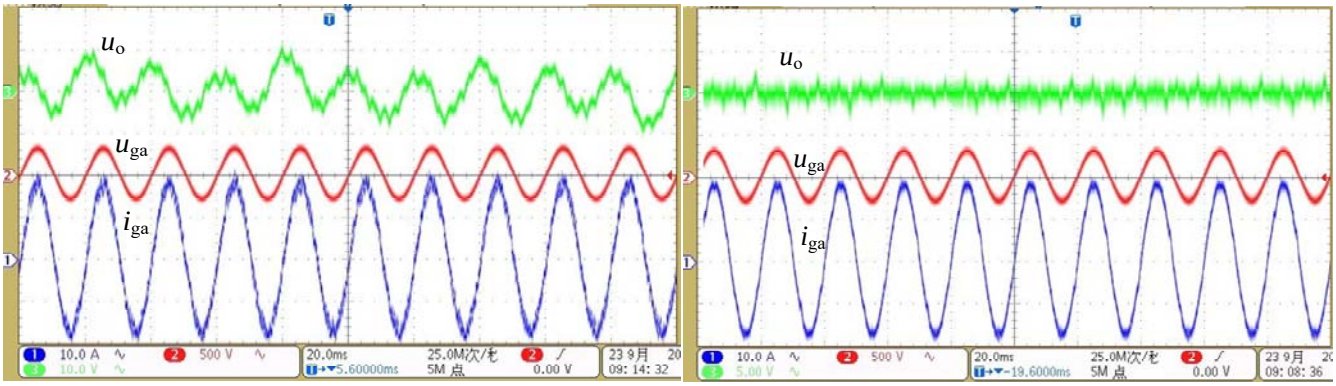

(a). MPDPC ***(b).MPDPC-VM***

Fig.18 Response of neutral point potential

6. CONCLUSION

Aiming at the defects of the traditional MPDPC strategy, such as large grid-connected current ripple and difficult selection of filter inductor due to the unfixed switching frequency, an improved model predictive control method considering inductance parameters mismatch with the combined voltage vector modulation-based scheme was proposed, which realized the balance control of neutral-point potential without additional weighting factor and eliminate the prediction tracking error caused by the model parameter mismatch. The validity and effectiveness of the new MPDPC-VM method have been confirmed through extensive simulation and experimental results. The results show that:

(1) The proposed MPDPC-VM increases the number of voltage vectors in each sampling period and significantly reduces the grid current ripple and harmonics;

(2) The reactive power changes with the reference quickly in 1ms with power ripple elimination. The experimental results demonstrate the feasibility of the MPDPC-VM. The dynamic performance of the MPDPC-VM is superior to the conventional MPC and linear control;

(3) Due to the introduction of virtual voltage vector, the optimization process is increased, but it can be solved by using advanced processing chips. In addition, this paper focuses on solving the problem of unfixed switching frequency when the traditional MPDPC-VM adopted;

(4) The inductance parameter identification based on MARS in this paper can effectively reduce the prediction tracking error and improve the parameter robustness of the system.

ACKNOWLEDGMENT

This work is supported by the Youth Project of Science and Technology Plan, Shaanxi Province(2022JQ-512), Postdoctoral Research Station in control science and engineering, Youth Enhancement Scheme of Xi'an Association for Science and Technology (095920201306) and State Key Laboratory of Electrical Insulation and Power Equipment of Xi'an Jiaotong University (EIPE21201), Applied technology R & D project (GX2106), Beilin District, Xi'an.

REFERENCES

[1] J. W. Kolar and T. Friedli, "The Essence of Three-Phase PFC Rectifier Systems—Part I," *IEEE T Power Electr*, vol. 28, no. 1, pp. 176-198, Jan. 2013, doi: 10.1109/TPEL.2012.2197867.

[2] Z. He et al., "A Novel Method to Evaluate the Influence of Vienna Rectifier Neutral-Point Voltage Fluctuation on Input Current Quality," *IEEE T Power Electer*, vol. 36, no. 7, pp. 8347-8358, Jul 2021, doi: 10.1109/TPEL.2020.3042251.

[3] C.L. Dang, X.Q. Tong, W.Z. Song, et al., "Cost Function based Modulation Scheme of Model Predictive Control for VIENNA Rectifier," IET Power Electronics, 2019, 12(14) 3646-3655 .

[4] C.L. Dang, F.Wang, D. Liu, et al., "Model Predictive Direct Power Control Scheme for Vienna Rectifier with Constant Switching Frequency," IET Power Electronics, 2021, 15(3): 216-225.

[5] X. Li, J.B. Wang, Q.H. Zeng, et al., "Direct Power Control of Vienna-Type Rectifier Based on Sliding Mode Variable Structure Control," *Electrical & Energy Management Technology*, 2015, 11(5): 1427-1434, doi: 10.16628/j.cnki.2095-8188.2015.08.013.

[6] Y.H. Zhou, A. Zhang, H.Zhang, et al., "A model predictive control with online inductance estimator for three-phase Vienna rectifiers," presented at the 46th Conf. IEEE Industrial Electronics Society, Singapore, October. 18-21, 2020.

[5] J. S. Lee, K. B. Lee, and F. Blaabjerg, "Predictive Control with Discrete Space-Vector Modulation of Vienna Rectifier for Driving PMSG of Wind Turbine Systems," *IEEE T Power Electr*, vol. 34, no. 12, pp. 12368-12383, Dec 2019, doi: 10.1109/TPEL.2019.2905843.

[6] X.Y. Sun, C.L. Dang, Z.H. Jiang, et al., "Mode Predictive Direct Power Control Scheme with Fixed Operation Frequency for a Vienna Rectifier Based on Voltage-Sensorless,"*IEEJ TRANSACTIONS ON ELECTRICAL AND ELECTRONIC ENGINEERING(Early Access)*

[7] Y.C. Zhang and W. Xie, "Low Complexity Model Predictive Control-Single Vector-Based Approach," *IEEE T Power Electr*, vol. 29, no. 10, pp. 5532-5541, Oct 2014, doi: 10.1109/TPEL.2013.2291005.

[8] S.E. Daoudi, L. Lazrak, M.A. Lafkih, "Upgraded sensorless direct torque control using MRAS-sliding mode observer for asynchronous motor," presented at the 6th Int. Conf. IEEE Optimization and Applications (ICOA), Beni Mellal, Morocco, Apr. 20-21, 2020.

[9] J. S. Lee, K. B. Lee, and F. Blaabjerg, "Predictive Control with Discrete Space-Vector Modulation of Vienna Rectifier for Driving PMSG of Wind Turbine Systems," *IEEE T Power Electr*, vol. 34, no. 12, pp. 12368-12383, Dec 2019, doi: 10.1109/TPEL.2019.2905843.

[10] Y. Yang, H.Q. Wen, and D.P. Li, "A Fast and Fixed Switching Frequency Model Predictive Control with Delay Compensation for Three-Phase Inverters," *IEEE Access*, vol. 5, pp. 17904-17913, Dec 2017, doi: 10.1109/ACCESS.2017.2751619.

[11] A. R. Izadinia and H. R. Karshenas, "Optimized current control of vienna rectifier using finite control set model predictive control," in *Proc. PEDSTC*, Tehran, Iran, 2016, pp. 596-601.

[12] J. S. Lee and K. B. Lee, "Predictive Control of Vienna Rectifiers for PMSG Systems," *IEEE T Ind Electron*, vol. 64, no. 4, pp. 2580-2591, Apr 2017, doi: 10.1109/TIE.2016.2644599.

[13] F. Donoso, A. Mora, R. Cardenas, A. Angulo, et al., "Finite-Set Model-Predictive Control Strategies for a 3L-NPC Inverter Operating With Fixed Switching Frequency," *IEEE T Ind Electron*, vol. 65, no. 5, pp. 3954-3965, May 2018, doi: 10.1109/TIE.2017.2760840.

[14] C.M. Zheng, T. Dragicevic, Z.B. Zhang, et al., "Model Predictive Control of LC-Filtered Voltage Source Inverters With Optimal Switching Sequence," *IEEE T Power Electr*, vol. 36, no. 3, pp. 3422-3436, Mar 2021, doi: 10.1109/TPEL.2020.3015540.

[15] C.l. Dang, X.Q. Tong, J.J. Huang, *et al*, "The neutral point-potential and current model predictive control method for Vienna rectifier," *J. Franklin Inst*, vol. 354, no. 17, pp. 7605-7623, Nov 2017.

[16] Y.Q. Mu, S.M. Guo, H.B. Zhu, et al, "Neutral Point Potential Balance Method of NPC Three-level Converter Combining Modulation Factor and Vector Selection," ASEMD, Tianjin, China ,2020,pp.1-2.

[17] Z,F, Liu， G.P, Du， F.F. Du, "Research status and development trend of finite set model predictive control in power electronic system,"*Acta Electrotechnics Sinica*,2017,**32**, (22),pp.58-69(in Chinese).

[18] P. Antoniewicz and M. P. Kazmierkowski, "Virtual-Flux-Based Predictive Direct Power Control of AC/DC Converters with Online Inductance Estimation," *IEEE T Ind Electron*, vol. 55, no. 12, pp. 4381-4390, Dec 2008, doi: 10.1109/TIE.2008.2007519.

[19] C. Gong, Y.H. Hu, J.Q. Gao, et al., "An Improved Delay-Suppressed Sliding-Mode Observer for Sensorless Vector-Controlled PMSM," *IEEE T Ind Electron*, vol. 67, no. 7, pp. 5913-5923, Jul 2020, doi: 10.1109/TIE.2019.2952824.

[20] X.Y. Li and R. Kennel, "General Formulation of Kalman-Filter-Based Online Parameter Identification Methods for VSI-Fed PMSM," *IEEE T Ind Electron*, vol. 68, no. 4, pp. 2856-2864, Apr 2021, doi: 10.1109/TIE.2020.2977568.

[21] W. Zhu et al., "A Novel Model Predictive Control Method with Discrete Space Vector Modulation for Neutral-Point Voltage Balancing of Vienna-Type Rectifier," in *Proc. ECCE*, Portland, United States, 2018, pp. 4051-4055.

[22] M. Hui, W. Li, Y.X. Xie, et al., "Research on direct power control based on sliding mode control for Vienna-type rectifier," presented at the 42nd Int. Conf. IEEE Industrial Electronics Society, Florence, 2016, pp: 25-30.

[23] J. S. Lee, K. B. Lee, and F. Blaabjerg, "Predictive Control With Discrete Space-Vector Modulation of Vienna Rectifier for Driving PMSG of Wind Turbine Systems," *IEEE T Power Electr*, vol. 34, no. 12, pp. 12368-12383, Dec 2019, doi: 10.1109/TPEL.2019.2905843.

[24] Z. He et al., "A Novel Method to Evaluate the Influence of Vienna Rectifier Neutral-Point Voltage Fluctuation on Input Current Quality," IEEE T Power Electr, vol. 36, no. 7, pp. 8347-8358, Jul 2021, doi: 10.1109/TPEL.2020.3042251.

[25] O. C. Kivanc and S. B. Ozturk, "Sensorless PMSM Drive Based on Stator Feedforward Voltage Estimation Improved With MRAS Multiparameter Estimation," *IEEE-ASME T Mech*, vol. 23, no. 3, pp. 1326-1337, Jun 2018, doi: 10.1109/TMECH.2018.2817246.

[26] X. Liu, D. Wang, and Z.H. Peng, "A Computationally Efficient FCS-MPC Method Without Weighting Factors for NNPCs With Optimal Duty Cycle Control," *IEEE-ASME T Mech*, vol. 23, no. 5, pp. 2503-2514, Oct 2018, doi: 10.1109/TMECH.2018.2866591.

[27] X. Liu, D. Wang, and Z.H. Peng, "A Computationally Efficient FCS-MPC Method Without Weighting Factors for NNPCs With Optimal Duty Cycle Control," *IEEE-ASME T Mech*, vol. 23, no. 5, pp. 2503-2514, Oct 2018, doi: 10.1109/TMECH.2018.2866591.

Declaration of Interest Statement

All the authors declared that they have no conflicts of interest to this work.We declare that we do not have any commercial or associative interest that represents a conflict of interest in connection with the work submitted.